Brake Blending and Torque Vectoring of Road Electric Vehicles: A Flexible approach based on Smart Torque Allocation.

Luca Pugi[a]*, Tommaso Favilli[a], Lorenzo Berzi[a], Edoardo Locorotondo[a], Marco Pierini[a]

[a]*Department of Industrial Engineering, University of Florence (DIEF), Florence, Italy*

*Corresponding Author: *luca.pugi@unifi.it*

Brake Blending and Torque Vectoring of Road Electric Vehicles: a flexible approach based on Smart Torque Allocation.

Abstract: Application of regenerative braking on electric vehicles have a large impact on several aspects of design, implemented functionalities and overall performances of road vehicles. In particular, multi-quadrant capabilities and improved control performances of modern electric drives can be fully exploited to improve vehicle efficiency, stability and overall environmental impact. Conventional, Mechanical friction brakes are currently devoted not only to stop the vehicle but also to the actuation of safety related mechatronics systems such as EBD (Electronic Braking Distribution), ABS (AntiBlockierSystem) and ESC/ESP (Electronic Stability Control/Program). The result is an over-actuated system of electrical (electric motors) and mechanical actuators (friction brakes), whose mixed, blended application has to be carefully optimized. In this work authors propose a simplified approach in which concept transferred from previous studies on high speed trains and autonomous vehicles are re-proposed and adapted in an innovative way to electric road vehicles.

***Keywords*: Vehicle Dynamics, Regenerative Braking, Mechatronics, Optimal Thrust, Torque Allocation**

Introduction: Electric Braking on Road Vehicles

The application of electric traction systems to road vehicles offers to designers a wide range of innovative opportunities, since electric motors present some interesting features respect to conventional Internal Combustion Engines (ICE) [1], [2].

Electric motors can be both speed or torque controlled quite precisely in wide operational ranges. Modern power drives allow an accurate torque control in near to standstill conditions [3]. Also, these systems enable a four-quadrant control of most diffused typologies of traction motors (e.g. induction, wounded or PM synchronous machines, reluctance-hybrid machines, etc.) [4], [5].

This substantially means that traction motors should be easily perform regenerative braking allowing to increase autonomy and efficiency of electric vehicles, by recovering a significant part of vehicle kinetic energy during the braking phase [6]. However, the vehicle's wheels should be equipped also with conventional dissipative brake (disc brake), in order to guarantee the minimum braking performance that ensure the required driving safety.

Wear and heating of friction brake pads is substantially proportional to dissipated energy [7], [8], so the availability of electric braking offers an important contribution also in improving maintenance costs and environmental impact (in terms of debris and other pollutants that are produced and diffused by worn brake materials). In particular, worn brake debris are credited as the most important source of pollution not related to combustion [9] and its toxicity effects are difficult to be completely quantified considering variety of involved chemical substances and complexity of the involved bio-physical interaction [10], [11].

The way in which electric motor's control is performed typically corresponds to a bandwidth [12] that is more than enough respect to actual need and specifications, not only for traction and braking systems but also of mechatronic devices (e.g. EBD, ABS or ESC-ESP) devoted to maintain vehicle stability and safety, not only during the braking phase but also during traction or cornering manoeuvres [13], [14].

Power to size ratio of electric units is relatively good so it's also feasible the usage of multiple traction motors to precisely distribute torque efforts to different wheels, assuring the possibility of implementing torque vectoring with all the corresponding advantages in terms of overall control of vehicle stability and performances. On these last topics there is wide literature, which is mostly referred to the particular case of a vehicle with four in-

wheel motors, that allow a complete control of longitudinal efforts exerted on each wheel [15]–[21].

As a consequence, current developments of EV's powertrain are imposing a strong synergy between electric traction-braking system and the conventional friction brake [22]–[24], not only to control vehicle longitudinal dynamics, but also in terms of lateral stability[12], [14]. The presence of multiple electric and braking units makes the vehicle an over-actuated system, in which the action of each actuator is constrained by fixed or variable physical limits:

- **Friction Brake Units**: are substantially constrained to work as passive components, able only to dissipate vehicle kinetic energy. Further thermal limitations concerning maximum dissipated energy have to be considered [25]–[27] (typically, power limitations are scheduled respect to temperature).
- **Electric Units**: performances of the system are constrained by thermal, current and power limitations of motors, power units and electric storage systems [28]. In particular, limitations in the braking phase should be more severe respect to the ones in the traction phase due to voltage/current limitations of the motor drive at very low speed. Also, the storage system has to be able to manage the recovered energy. Limitations due to energy storage system are strongly influenced by state of charge (SOC) and health (SOH) of accumulators.

The way in which the action of both conventional and electric braking system is merge, optimized and controlled is typically called **Brake Blending** [29], [30]. Considering the over-cited interactions of brakes with almost all the mechatronics subsystems that assure vehicle stability and safety [31], the action of the brake blending has to be "transparent" for the user: controller have to be able to compensate different performances and

availability levels of electric and conventional actuators, maintaining a known stable behaviour of the vehicle.

Objectives and Innovation Content of the Proposed Work

In a previous work [32], authors develop a simple EV Real-Time (RT) plant and relative subsystem, in order to verify the validity of the modelling process.

Aim of this paper is to transfer and merge in an original way a wide know-how, taken from different sectors and previous experiences ranging from robotics to vehicle engineering, in order to optimize blending and optimal torque allocation of electric and conventional friction brakes on road vehicles.

In particular, authors intend to present a general flexible simulation methodology that can be easily adapted to different vehicle powertrains and brake plants using simple modular models that can be reassembled and customized according the considered use-cases. The proposed models are optimized for fixed step integration, in order to make easier Real Time Simulation RTS (both for fast prototyping and Hardware In the Loop HIL and Software In the Loop SIL testing) and co-simulation (integration of proposed brake and control models with other more complex ones provided by external industrial partners). Non-secondary advantages of the proposed approach are Model Partitioning for Multi-Thread Execution, improved model interoperability and computational efficiency of the model.

General Structure of the Brake Model with Integrated Brake Blending Controller

In Figure 1 it's introduced a simplified scheme of the proposed approach: all the brake plant is supposed to be controlled by a "brake demand" which is an abstraction of a digital or physical signal (as example the brake booster output pressure), which corresponds to

a braking torque reference produced by a human or an autonomous driver of the car. These brake demand should be further modified by on-board mechatronics subsystems such as EBD, ABS and ESP in order to improve vehicle stability and safety. Resulting brake demand is a vector of brake reference torques, whose scalar components are the Tq_{ref_i}, each one representing the actuation of the i-th vehicle wheel.

As visible in Figure 1, *Unifi Brake Model (UBM)* is composed by three sub-modules:

- Brake Blending: an algorithm which control and execute the brake blending strategy;
- Brake Plant: a model devoted to control and actuate the braking units;
- Braking units.

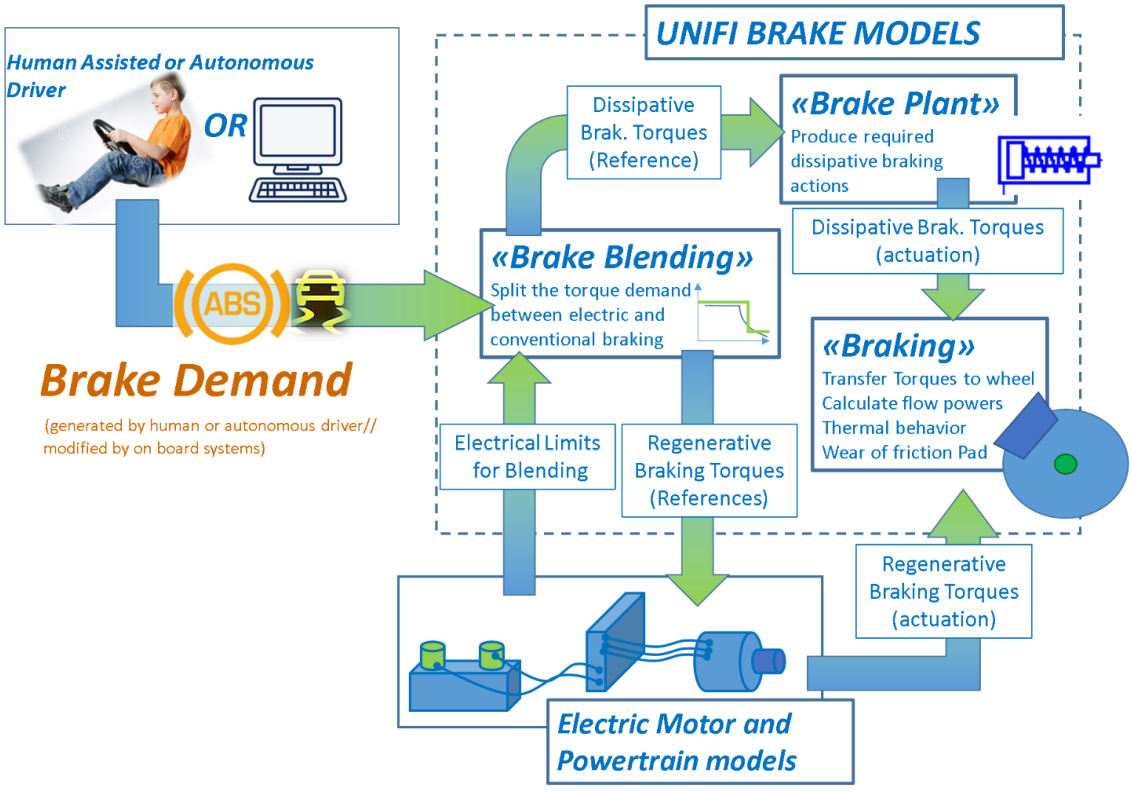

Figure 1 General layouts and interactions of the UBM with other vehicle subsystems

Brake Blending Controller

Brake demand, generated by the driver and modified by the stability controller, is processed by a Brake Blending Controller (BBC) that have to decide how to split the torque demand between the conventional brake and the regenerative one generating the corresponding references $Tq_{ref\_br\_i}$ and $Tq_{ref\_reg\_i}$, according to (1). In this way the resulting controller is quite simple and all the functions concerning the stability of the vehicle are completely managed by upper level controllers, that are traditionally devoted to this task.

$$Tq_{ref\_i} = Tq_{ref\_br\_i} + Tq_{ref\_reg\_i} \tag{1}$$

Main component of BBC logic for a single motorized wheel is represented in Figure 2:

a) *Torque Limitations*: according to the state of the motor and of the energy storage systems the BBC evaluates the drivetrain performance limitations, in terms of maximum (for traction phase) and minimum (for braking phase) deliverable torque, as function of power and current that are tolerable by the electric powertrain, automatically selecting the most cautious/restrictive condition. Currently these electrical limitations are supposed to be read from an external vehicle data bus and calculated by the corresponding interested control units (battery BMS, and/or motor driver).

b) *Torque Demand Generation*: according brake and traction commands performed by vehicle driver, a corresponding reference torque demand Tq_{ref_i} is evaluated.

c) *Electrical Torque Saturation*: in order to maximize the usage of regenerative brake respect to conventional brakes, the torque reference is supposed to be entirely exerted by electric motors. Generated torque reference is saturated respect to the known limitations of the electric plant previously calculated (*a*), producing a corresponding regenerative torque reference $Tq_{ref\_reg\_i}$. It's interesting to notice that these that is torque limitations should be used also to model some specific features of the

powertrain. As example if the wheel is not motorized the saturation is set to a null value. On the other hand, classic powertrain solutions can be easily modelled imposing mutual constraints between the torque exerted by the two connected wheels. In particular, for an ideal differential gearbox, both outputs torque are equals, so connected wheels should be saturated to a common minimum allowable value.

d) *Braking Torque Demand Calculation*: since the response of electric actuators is saturated respect to their known limits, in order to satisfy the required brake torque demand, the difference between desired braking torque and the one made available by regenerative braking become the desired amount of braking torque that have to be delivered to the wheel by the conventional/mechanical brake system, in order to compensate the limitations (a) of the electric brake plant, according to (1).

e) *Dynamic Compensation*: since electric and mechanical brake plant should have a quite different dynamical behaviour (specifically, it's supposed a faster electric plant), additional signal calibration filter, implemented in terms of transfer function, should be applied to the electric braking torque reference, in order to compensate its faster behaviour and to avoid undesirable noise in the braking torque references generation.

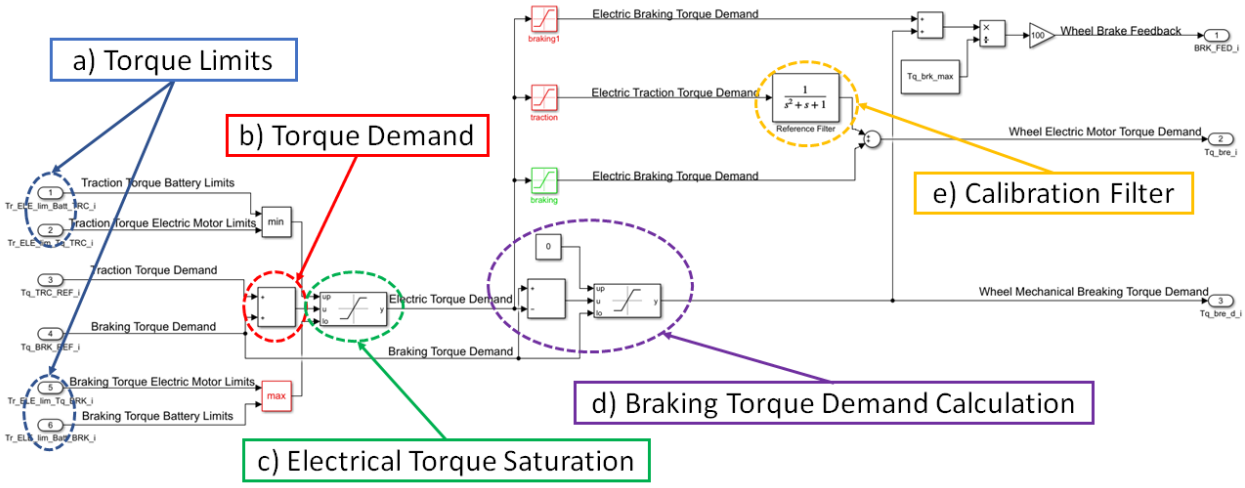

Figure 2 Equivalent implementation in MATLAB Simulink™ (tested releases 2017a-2018b) of the BBC.

Integration of Brake Blending within Vehicle Stability Controllers

BB logic previously described by the scheme of Figure 2 assures an optimal allocation of electric regenerative efforts respect to conventional braking, with the intent to maximize the recovered energy, by taking the full advantage of the electric actuator. However, in modern applications, braking system is not only devoted to control vehicle longitudinal dynamics: a fast differential application of braking torques among wheels is typically used to correct the directional behaviour of the vehicle. Stability controllers like ESP™ [33] perform vehicle torque vectoring by modulating the braking efforts applied on left and right wheels, in order to produce a desired correction torque M_{yaw} (2), where y_i is the vehicle half-track of the i-th wheel and r_w the corresponding rolling radius. With $Tq^*_{ref\_i}$ we indicate the torques desired on each wheel, and with Tq_{ref_i} the one who's really applied on them by the actuator.

$$M_{yaw} = \sum_{i=1}^{n=4} \frac{Tq^*_{ref\_i} - Tq_{ref\_i}}{r_w} y_i \tag{2}$$

An optimal BB strategy also corresponds to an optimal torque allocation, so authors also investigate this aspect as a part of the integration of the brake blending controller within the lateral stability one [28]–[31].

The main focus of this work it's not to further investigate the best way in which a EV cornering or lateral stability's control can be implemented, but only find a very simple and efficient way to produce a good allocation of torques on wheels aimed at maintaining vehicle stability while maximizing the recovery of kinetic energy during braking phase, which is significantly a lower layer of the over-cited control stability algorithm [34], [35]. In this work authors consider a simple general torque vectoring approach, supposing that applied longitudinal F_{ref_i} (3) efforts can be modulated separately on each wheel, being the force calculated as ratio between torques Tq_{ref_i} and corresponding wheel rolling

radius r_w. Also, transversal distances y_i between tyre contact patches and vehicle symmetry plane are supposed to be constant and completely known as visible in Figure 3.

Finally, in the calculation it's completely neglected the contribution of steering angles whose typical values in normal operating conditions are lower than 0.1-0.12 rad (about 6°-7°).

$$F_{ref\_i} = \frac{Tq_{ref\_i}}{r_w} \tag{3}$$

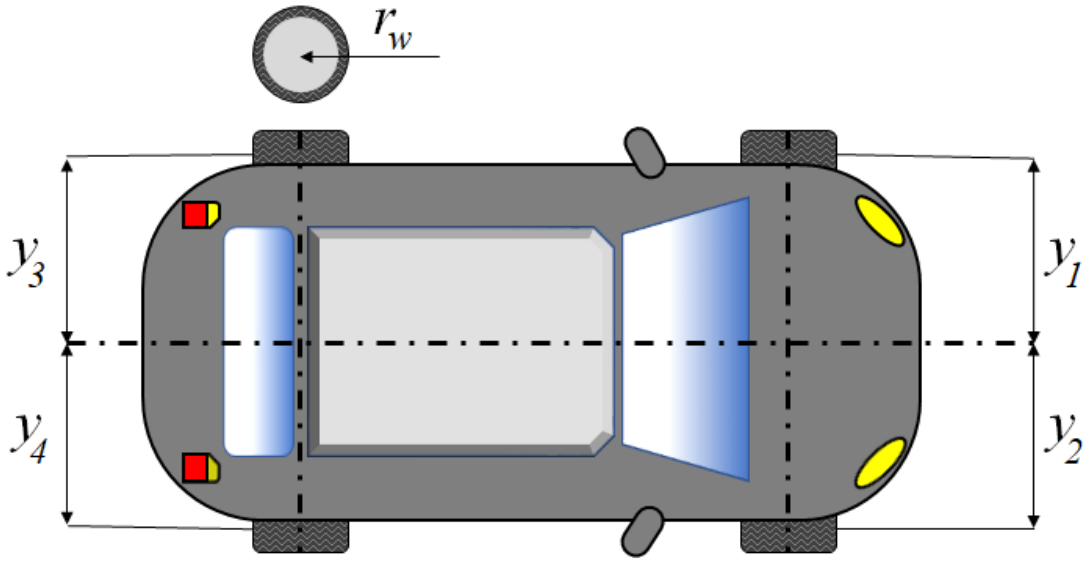

Figure 3 simplified vehicle layout adopted to describe brake blending integration in vehicle stability controllers

Considering over-cited simplifications, the system is clearly over-actuated as seen in eq. (2), since four different efforts can be regulated. In order to find a near to optimal solution authors considered some constraints that have to be respected.

First, total braking or traction demand should not be affected by the action of the stability controller, so the exerted torques Tq_{ref_i} has to be maintained as unaltered as possible respect to $Tq^*_{ref\_i}$, being the latter the torques that should be applied to wheels without any intervention of the stability controller, as visible in (4).

$$Tq^*_{ref\_i} - Tq_{ref\_i} \cong 0 \quad \forall i = 1,2,3,4 \tag{4}$$

Values of applied torque T_{ref_i} have to be limited according on available braking and traction performance T_{min_i} and T_{max_i}, which can be scheduled respect to motor shaft speed (which must be controlled in order to perform the motor ideal traction characteristic [34] of Figure 4, and availability of the energy storage system, by (5).

$$Tq_{\min\_i} \le Tq_{ref\_i} \le Tq_{\max\_i} \tag{5}$$

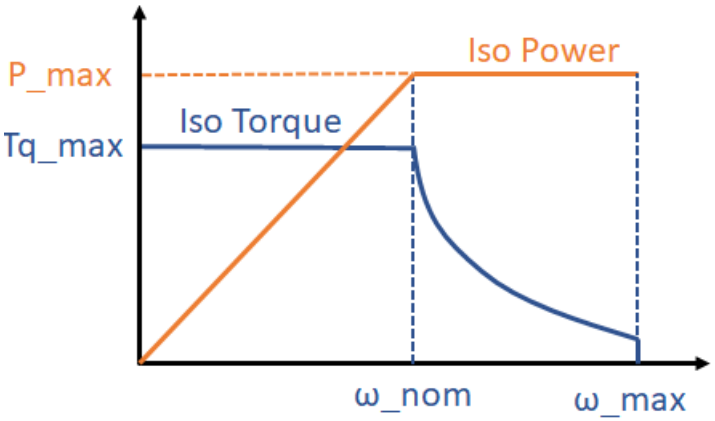

Figure 4 Motor ideal traction characteristic

It should be noticed that for vehicles with independent in-wheel motors also traction efforts on each wheel can be modulated independently; so, sign of $T_{\min\_i}$ and $T_{\max\_i}$ can be different.

Finally "norm 2" of the applied correction torque (4) has to be minimized (6), being Tq_{ref_i} the torque applied on the corresponding i-th wheel:

$$\left\| Tq_{ref\_i} - Tq_{ref\_i*} \right\|_2 = \left(\sum_{i=1}^{n=4} \left(Tq_{ref\_i} - Tq^*_{ref\_i} \right)^2 \right)^{\frac{1}{2}} \tag{6}$$

In this way the corrections torques (6) are distributed between actuators, improving reliability and energy consumptions. Also, minimization of (6) contributes to find a solution that is reasonably far from constraints and limitations described by (5). A solution which is far from constraint should finally produce a smoother dynamical behaviour of applied actuations, since a saturation of one or more efforts should produce a discontinuous behaviour across constraints.

Authors also propose a numerical implementation of the method, which involves the usage of limited numerical resources that are more than affordable for an industrial RT application. Proposed implementation is described by following steps.

First conditions corresponding to relations (2) and (4) are implemented obtaining the linear system (7).

$$\overbrace{\begin{bmatrix} -\frac{y_1}{r_w} & \frac{y_2}{r_w} & -\frac{y_3}{r_w} & \frac{y_4}{r_w} \\ 1 & 1 & 1 & 1 \end{bmatrix}}^{} \begin{bmatrix} {}_{ef\_1} - Tq^*_{ref\_1} \\ Tq_{ref\_2} - Tq^*_{ref\_2} \\ Tq_{ref\_3} - Tq^*_{ref\_3} \\ Tq_{ref\_4} - Tq^*_{ref\_4} \end{bmatrix} = \begin{bmatrix} M_{yaw} \\ 0 \end{bmatrix} \tag{7}$$

By solving (7) using the Moore-Penrose Pseudo-Inverse matrix of A it's possible to calculate the desired torque correction applied on every wheel. The usage of Pseudo-Inverse assures the minimization of the norm 2 of the solution, automatically involving the respect of condition (6). It should be also easily demonstrated that considering the typical symmetry properties of vehicle layouts ($|y_1|=|y_2|$; $|y_3|=|y_4|$) the minimization of the norm 2 of the performed correction automatically assure the respect of condition (6). Also system (7) can be rewritten removing the second row from matrix A, resulting in the even simpler formulation (8).

$$\overbrace{\begin{bmatrix} -\frac{y_1}{r_w} & \frac{y_2}{r_w} & -\frac{y_3}{r_w} & \frac{y_4}{r_w} \end{bmatrix}}^{} \begin{bmatrix} {}_{ef\_1} - Tq^*_{ref\_1} \\ 1q_{ref\_2} - Tq^*_{ref\_2} \\ Tq_{ref\_3} - Tq^*_{ref\_3} \\ Tq_{ref\_4} - Tq^*_{ref\_4} \end{bmatrix} = M_{yaw} \tag{8}$$

Considering equal transversal distances of wheels respect to symmetry plane ($|y_1|=|y_2|=|y_3|=|y_4|$) the corresponding solution (9) is even simpler and can be solved manually.

$$\begin{bmatrix} Tq_{ref\_1} - Tq^*_{ref\_1} \\ Tq_{ref\_2} - Tq^*_{ref\_2} \\ Tq_{ref\_3} - Tq^*_{ref\_3} \\ Tq_{ref\_4} - Tq^*_{ref\_4} \end{bmatrix} = \begin{bmatrix} -M_{yaw} \frac{r_w}{4y_i} \\ M_{yaw} \frac{r_w}{4y_i} \\ -M_{yaw} \frac{r_w}{4y_i} \\ M_{yaw} \frac{r_w}{4y_i} \end{bmatrix} \tag{9}$$

More generally, the calculation of a pseudo-inverse matrix of A it's relatively easy considering the small size of the matrix.

Once solution of (7) is calculated, it's possible to impose to each torque profile T_{ref_i} the saturation constrain (5). Solution of (7) is then recalculated imposing for each saturated T_{ref_i} the corresponding saturation values calculated according (10).

$$\begin{cases} if\,(Tq_{ref\_i} > Tq_{\max\_i}) \Rightarrow Tq_{ref\_i} = Tq_{\max\_i} \\ if\,(Tq_{ref\_i} < Tq_{\min\_i}) \Rightarrow Tq_{ref\_i} = Tq_{\min\_i} \end{cases} \tag{10}$$

As example, if T_{ref_3} is limited to $T_{\max\_3}$, calculation of (7) is repeated solving system (11) , in which the value of the third element is locked to the corresponding saturated value.

$$\overbrace{\begin{bmatrix} -\frac{y_1}{r_w} & \frac{y_2}{r_w} & -\frac{y_3}{r_w} & \frac{y_4}{r_w} \\ 1 & 1 & 1 & 1 \end{bmatrix}}^{} \begin{bmatrix} {}_{ef\_1} - Tq^*_{ref\_1} \\ Tq_{ref\_2} - Tq^*_{ref\_2} \\ Tq_{\max\_3} - Tq^*_{ref\_3} \\ Tq_{ref\_4} - Tq^*_{ref\_4} \end{bmatrix} = \begin{bmatrix} M_{yaw} \\ 0 \end{bmatrix} \tag{11}$$

Calculation is then repeated until a valid solution is found or alternatively when every torque profile T_{ref_i} is saturated. The resulting method is quite efficient, since in the worst case four iterations are needed. From a computational point of view, the most demanding task is represented by the inversion of the A matrix; however, as number of computational steps increase from one to four, also the size of the problem decreases, further reducing the corresponding computational load.

Current implementation should be further improved scaling the prescribed correction of torque profiles Tq_{ref_i}-$Tq^*_{ref\_i}$ respect to the corresponding normal loads applied to wheels.

However, this further optimization of torque allocation should be useful only for vehicles in which there is a strong load unbalance between wheels.

Brake Plant

Brake Plant Model has to reproduce the behaviour of a real brake plant model, intended as the system which converts the brake demand (produced by the driver and corrected by various on-board subsystem) in real clamping forces of brake pads, able to produce the desired brake torques on wheels.

Brake plants currently adopted on road vehicles are mainly fluidic servo-amplification and actuation systems as visible in schemes of Figure 5 [28]:

- *Hydraulic plants*: for small to medium size vehicles (motorcycles, cars and light vans/trucks).
- *Pneumatic plants*: for heavy, large or articulated vehicles (trucks). This plant scheme is very similar to the UIC pneumatic brake plant also adopted on railway vehicles [36],[37].

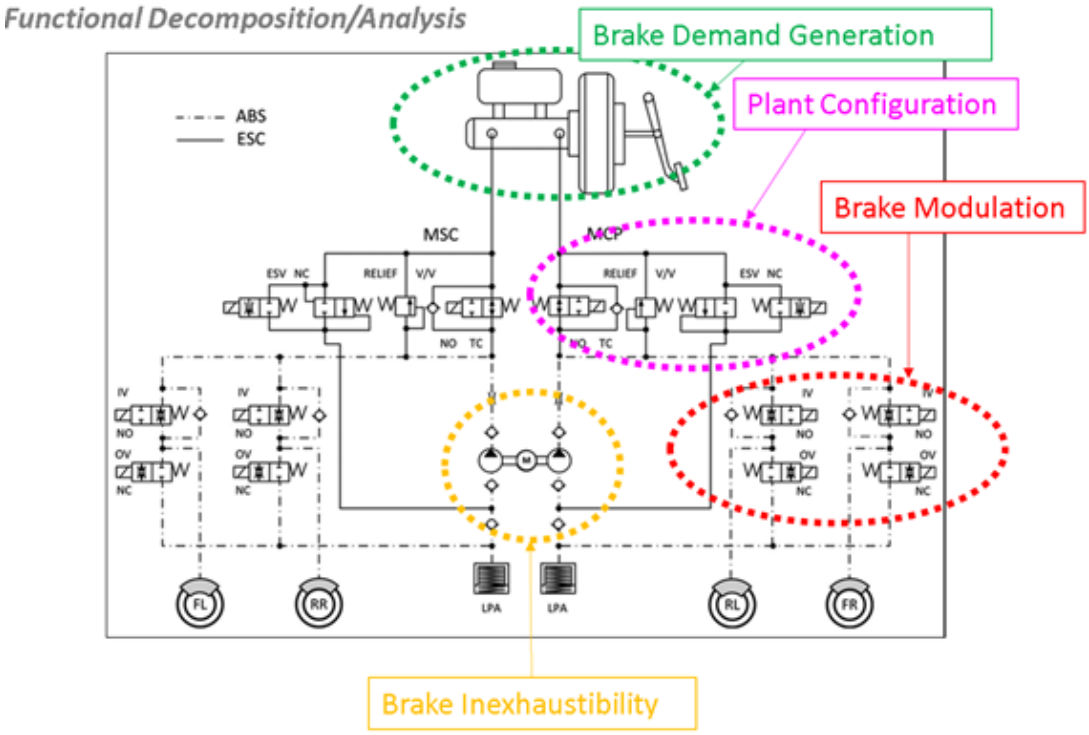

Figure 5 Functional decomposition of a hydraulic braking plant of a car [28].

Respect to schemes of Figure 5, brake plant is analysed in terms of functions that are performed by different subsystems and then translated in an equivalent functional model, visible in Figure 6.

Adopted model reproduce only some limited physical features of the simulated plant:

- **Brake Demand Generation:** it's simulated as a converted and servo-amplified command signal which represents a clamping force reference and consequently a torque one. For modelling purpose this stage is considered a servo-amplification performed by a nonlinear amplifier with limited bandwidth.
- **Plant Configuration:** driver brake demand and plant configuration are affected by mechatronics subsystems, such as ABS or ESP/ESC, that have to modulate the torque applied to wheels in order to preserve vehicle safety and stability. All these functionalities are simulated in a simplified way by assuring the possibility of a direct access of external commands, from on board systems, by the valves that control the brake clamping units. According the current plant state, applied friction brake

commands (i.e. conventional braking or correction imposed by ABS/ESP systems) are filtered by transfer functions (second order filters), that could be customized in order to reproduce the response of corresponding fluid components (limited bandwidth).

- **Brake Modulation:** clamping pressure applied to brakes is typically regulated by electro-hydraulic valves. The latter are able to connect the controlled actuator with a pressure source or to discharge it in a tank in function of the regulation strategy adopted by upper level control layers. A single effect actuator controlled by a 3/3 valve (three ways, three states valve) is the best way to approximate the plant response.
- **Brake Inexhaustibility:** safety of brake plant involves the availability of supply pressure in every working condition. This feature is important for mechatronics systems, like ABS and ESP, whose fluid consumptions are difficult to be evaluated, especially when complex regulation patterns are involved. Brake torques have to be modulated also when it's not performed a braking manoeuvre by the driver, as example assisted braking or brake patterns to preserve vehicle stability on a curve. Real plants have additional capacities and feeding/pumping units to assure pressurization in almost every condition.

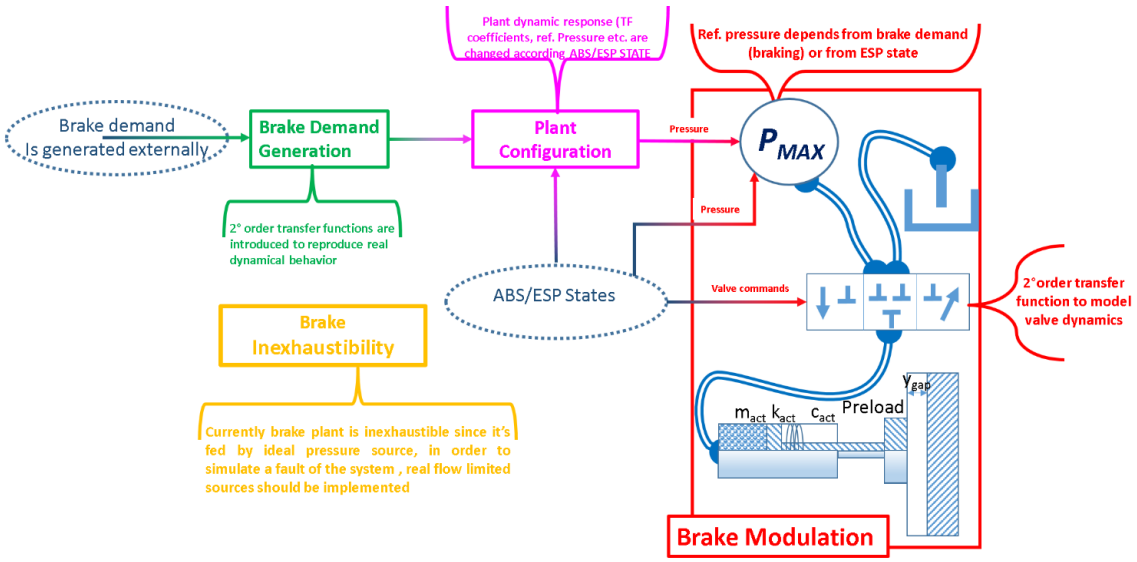

Figure 6 functional model of the brake plant adopted in this work.

Sketches and Equations of Brake Modulation Sub-model

Respect to conventional models available in literature authors focused their attention on his numerical stability for fixed step Real Time Implementation (RTI): this is an issue often under-evaluated, since the integration of hydraulic systems (highly computational stiff) is easily performed on commercial codes with variable step solvers, that are almost unsuitable for RTI in which fixed step implementation is almost mandatory.

For implementation of the model scheme of Figure 6, authors started from the integration of (12) in order to calculate pressure inside the brake actuator chamber [38].

$$\begin{cases} \dfrac{dp}{dt} = \beta\left[\dfrac{1}{\rho}\dfrac{d\rho}{dt} + \alpha\dfrac{dT}{dt}\right] = \beta\left[-\dfrac{1}{v_s}\dfrac{dv_s}{dt} + \alpha\dfrac{dT}{dt}\right] \\ \beta = \dfrac{\rho}{\left(\dfrac{\partial\rho}{\partial p}\right)_T} = \dfrac{1}{v_s\left(\dfrac{\partial\rho}{\partial p}\right)_T} = \dfrac{-v_s}{\left(\dfrac{\partial v_s}{\partial p}\right)_T} = -\dfrac{v_s}{v_{s0}}\dfrac{1}{\left(a_{p1} + 2a_{p2}\left(p-p_0\right) + a_{pt}\left(T-T_0\right)\right)} \\ \alpha = -\dfrac{1}{\rho}\left(\dfrac{\partial\rho}{\partial T}\right)_p = \dfrac{1}{v_s}\left(\dfrac{\partial v_s}{\partial T}\right)_p = \dfrac{v_{s0}}{v_s}\left(a_{t1} + 2a_{t2}\left(T-T_0\right) + a_{pt}\left(p-p_0\right)\right) \end{cases} \quad (12)$$

Force applied to calliper are proportional to internal pressure of the actuator whose dynamics is described by equation (13).

$$\underbrace{\qquad\qquad}_{\text{hit an endrun: } y\le y_{min} \text{ or } y\ge y_{max}} \underbrace{\qquad\qquad}_{\text{intererference with pad: } y\ge y_{max}} P_1 area \quad (13)$$

Equation (13) is used only to model the motion of the piston calliper: once the pad reach the surface of the brake disc ($y \le y_{min}$ *or* $y \ge y_{max}$) derivatives of position y are set to zero and maximum run is saturated to y_{max}. Clamping force is then calculated solving a static problem since the state derivatives are neglected. The main advantage of this approach is to avoid the application of contact stiffness/damping terms, which often introduce high frequency poles that are difficult to be handled by fixed step solvers running at low

frequencies (no more than 1 kHz). This is a specific numerical trick that author have successfully applied for this application, drastically improving stability of the system with low integration frequencies or ill/poor conditioned parameters.

Neglecting thermal terms in (12), pressure derivative are mostly function of specific volume/density of the fluid. Chamber volume V and its derivatives (14) are substantially known from kinematics, calculated according (13).

$$V = V_0 + Area\ y \Rightarrow \dot{V} \qquad (14)$$

On the other hand mass m inside the volume V of the actuator can be easily calculated by integrating the mass balance equation (15), where mass flow $\dot{m}$ sources due to valves (Q_{valves}) are calculated according (16).

$$\dot{m} \qquad \Rightarrow m(t) = m_0 \int_0^t Q_{valves} dt \qquad (15)$$

$$\begin{cases} Q_{valve} = h_x x \sqrt{|\Delta P|} \\ -1 \le x \le 1 \\ \Delta P = (P - P_{\max})(x \ge 0) + (P - P_{atm})(x < 0) \end{cases} \qquad (16)$$

P_{max} is the reference pressure to which are fed the brake units. During a brake manoeuvre is proportional to driver brake command. When the brake is activated by safety related system during a traction/coasting manoeuvre, instead, P_{max} is a fixed value decided by control logic state.

Real brake modulation valves have a finite response bandwidth. This feature is reproduced in this work by inserting a second-order filter function between input of the valve i_{valve} and the corresponding valve state x (17):

$$\frac{x}{i_{valve}} = \frac{\omega_n^2}{s^2 + 2\xi\omega_n s + \omega_n^2} \qquad (17)$$

Brake modulation valves are not the only components of a modern brake plant: according specific features of the simulated system, there is the need of simulating furthermore complex state-dependent functionalities. In order to fit all these features without increasing too much the number of integrated states and the overall complexity of the model, authors implemented the second order transfer function (17) as a variable coefficient system, in which valve response parameters such as pulse ω_n and damping coefficient ξ can be modified without producing discontinuities in the response. In this way a complex high order nonlinear system is approximated by a low-order one (2^{nd} order in this case), whose parameters are piece-wise gain interpolated respect to known plant and vehicle states.

This is a solution that authors have proven successfully in Hardware in the Loop (HiL) testing of pneumatic railway brakes [36]. In fact, even in that case there was the necessity of minimizing integrated states respect to a wide variety of different kind of responses that have to be simulated.

Braking Unit Model

Aim of the "Braking Unit Model" subsystem is to simulate the application of both regenerative/electric and dissipative/mechanical torques to wheels. In this way, we are able to calculate power flows and corresponding energy integrals. Knowing the amount of dissipated energy on each wheel, we can roughly calculate corresponding thermal and wear behaviour of brake friction components (pads and discs). Since brake friction factor depends from thermal and loading conditions, values of applied torques and dissipated energies should be corrected considering fading or more generally load-sensitivity of pads behaviour. So, the Braking Units subsystem satisfies the objective of calculating the performances of brake blending strategies, in terms of: (1) efficiency, (2) safety and (3) improved environmental impact, considering even the volume of pollutant debris

produced by wear of brake pads.

The system in question performs the following sub-functionalities, that are described in the scheme of Figure 7:

•Estimation of the thermal behaviour of components: temperature of components is calculated.

• Estimation of the wear of components: model evaluates wear and volume of pollutant debris produced in the braking phase.

•Stability of friction-braking performance: torques applied to wheels are corrected taking count of the thermal behaviour of friction components and the friction load sensitivity of the contact surface between discs and pads.

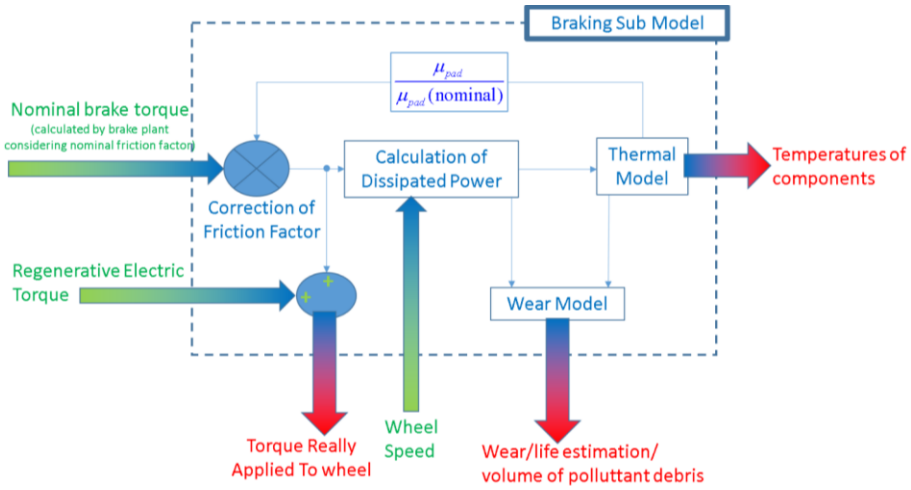

Figure 7 braking unit model and corresponding sub-models

Thermal Model of Braking Unit

Tq_Br_d_i and *w_w_i* are respectively the dissipative torque applied on the *i-th* wheel and the corresponding rotational speed. Dissipated power on brake-components *W_Br_d_i* is calculated according (18).

$$W\_Br\_d\_i = Tq\_Br\_d\_i \bullet \tag{18}$$

Energy is dissipated in the contact interface between pads and discs, so generated heat is transferred to both ones, being Q_{pad_i} and Q_{disc_i} respectively the heat flows transferred to pads and disc of the *i-th* wheel.

It's possible to define a heat flux distribution coefficient γ (19) in order to roughly evaluate how transferred heat flow is divided between pads and discs. By adopting the dimensionless coefficient γ, a decoupling of the two thermal systems (pads and the disc) is introduced. However, this is an approximation commonly accepted in literature [37].

$$\gamma = \frac{Q_{disc\_i}}{Q_{pad\_i}} \tag{19}$$

$$Q_{disc\_i} = \frac{\gamma}{\gamma+1} W_{br\_d\_i}; \quad Q_{pad\_i} = \frac{1}{\gamma+1} W_{br\_d\_i}; \tag{20}$$

Once inlet heat flows for each brake component are calculated according to (20), it's possible to perform a rough evaluation of mean temperatures T_{disc_i} (for disc) and T_{pad_i} (for pad), solving corresponding lumped systems, described by (21) and (22).

$$Q_{disc\_i} = C_{disc\_i} \dot{T}_{\_} \left(\overbrace{h_{conv\_d\_i}} + \overbrace{h_{cond\_d\_i}} + \overbrace{h_{rad\_d\_i}} \right) \left(T_{disc\_i} - T_{amb} \right) \tag{21}$$

$$Q_{pad\_i} = C_{pad\_i} \dot{T}_{\_} \left(\overbrace{h_{conv\_p\_i}} + \overbrace{h_{cond\_p\_i}} + \overbrace{h_{rad\_p\_i}} \right) \left(T_{pad\_i} - T_{amb} \right) \tag{22}$$

Cooling coefficients adopted in (21), (22) and also in the calculation of the heat distribution factor γ (19) should be tabulated respect to relevant physical parameters (component temperature, disc angular speed, vehicle speed, etc.). In this work these values are considered constants (e.g. a value of γ equal to 4,5 is considered), except for the convective term h_{conv}, whose value is scheduled in function of vehicle longitudinal speed.

Wear Model of Braking Unit

The volume of consumed friction components (disc brakes and pads) it's calculated according an Archard approach corresponding to equation (23), in which it's supposed a proportionality of worn volumes of pads and discs (V_{pad}, V_{disc}) respect to dissipated energy (E_d) on brake friction elements.

$$\left.\begin{aligned} V_{pad} &= k_{pad} E_d; \\ V_{disc} &= k_{disc} E_d; \end{aligned}\right\} \Rightarrow V_{debris} = \left(k_{disc} + k_{pad}\right) E_d; \tag{23}$$

Wear coefficients k_{pad} and k_{disc} are supposed known and constant. This is a clear approximation respect to more recent studies that shown a dependency of wear rates respect to temperature and clamping pressures [39].

However the main objective of the calculation (23) is to roughly evaluate the volume of pollutant debris (V_{debris}) derived by conventional braking, in order to evaluate how electric regeneration can produce a reduction in the production of harmful micro-particles. For this purpose relation (23) is very conservative, since recent studies have proved that higher braking temperatures are associated to a significant increase of the production rate of potentially dangerous micro-particles [40], [41].

Proposed Benchmark Vehicle

Proposed approach was tested on a virtual model of a benchmark vehicle, whose main parameters have been inspired by a known existing one. Main data are freely available on line [42]. However, latter were not enough to correctly compile and validate the proposed model. So, to completely exploit the system, the model was completed considered a parameter set that was considered reasonable respect to aims of the proposed study, derived by heuristic considerations. It's important to note that this is not a validated

model of specific vehicle, but a feasible benchmark with roughly near to realistic features.

Main geometric parameters of the vehicle are described in Figure 8 and TABLE I.

Additional data concerning brake, traction and power management systems are briefly described in TABLE II and TABLE III.

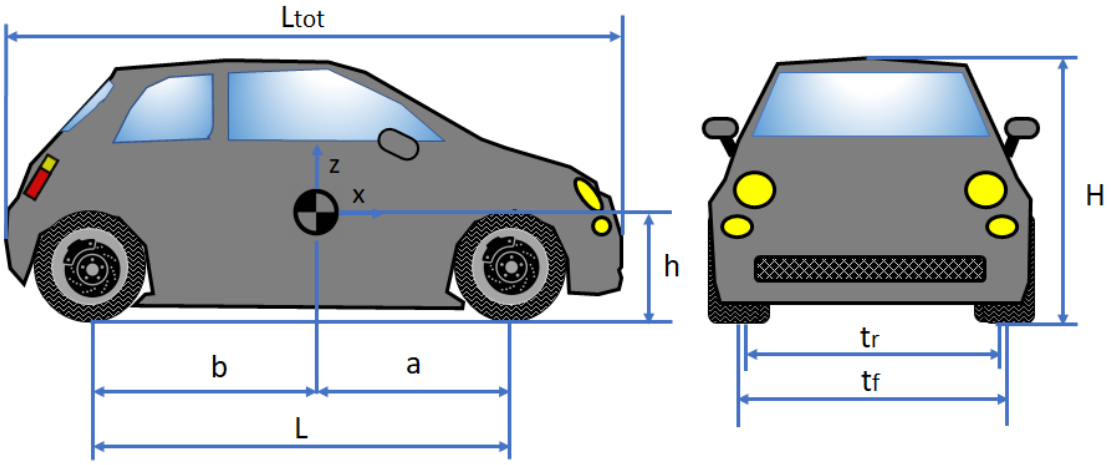

Figure 8 main geometrical parameters adopted for the benchmark test vehicle

TABLE I Main Inertial and Geometric Parameters of the Vehicle

Definition	***Symbol***	***Value***	***Source***
Total Length	L_{tot}	3,617 [m]	[29]
Wheelbase	L	2,300 [m]	[42]
Distance Front Axle-CM[X]	a	0,989 [m]	≠
Distance Rear Axle-CM[X]	b	1,311 [m]	≠
Height Ground-CM[X]	h	500 [mm]	≠
Front Track	t_f	1,407 [m]	[42]
Rear Track	t_r	1,397 [m]	[42]
Yaw Inertia	I_{zz}	1500 [kgm^2]	≠
Wheel Radius[Z]	r_w	0,283 [m]	≠
Vehicle Weight	M_v	1355-1800 [kg]	[29], ≠
Aerodynamic Drag	C_d	0,311 [%]	≠
Aerodynamic Lift	C_l	0,1	≠
[X]: CM is the acronym of Vehicle Centre of Mass			
[Y]: Depending on vehicle loading conditions			
[Z]: Mean equivalent rolling radius of tyres			
≠ this data has been extrapolated /supposed by authors through heuristic engineering consideration			

TABLE II Main Geometric and Thermal Parameters of the Vehicle's Brake System

Definition	***Symbol***	***Value***	***Source***
Front Disc ext. Radius	$R_{Disc,f,e}$	0,142 [m]	[42]
Rear Disc ext. Radius	$R_{Disc,r,e}$	0,125 [m]	[29]
Disc int. Radius	$R_{Disc,i}$	0,0305 [m]	[29]
Front Disc Thickness	$S_{Disc,f}$	0,022 [m]	[29]
Rear Disc Thickness	$S_{Disc,r}$	0,011 [m]	[29]
Disc Mass Density	ρ_{Disc}	7230 [kgm^{-3}]	≠
Disc Thermal Conductance	k_{Disc}	4170 [$Wm^{-1}K^{-1}$]	≠
Disc Specific Heat	C_{disc}	460 [$JKg^{-1}K^{-1}$]	≠
Pad Length-Height-Width	L_{pad}-H_{pad}-S_{pad}	0,11-0,55-0,014 [mm]	[29]
Pad Mass Density	ρ_{pad}	2030 [kgm^{-3}]	≠
Pad Thermal Conductance	k_{Pad}	174 [$Wm^{-1}K^{-1}$]	≠
Pad Specific Heat	C_{pad}	460 [$JKg^{-1}K^{-1}$]	≠
ABS Valves Bandwidth	ω_{hyd}	75 [rad/s]	≠

TABLE III Main Parameters of the Vehicle's Electric Powertrain and Power Management System

Definition	***Symbol***	***Value***	***Source***
Power of Traction Motor	P_{EM}	85 [kW]	[29]
Nom. Speed	$\omega_{EM(nom)}$	4000 [rpm]	[29]
Stall Torque	$Tq_{EM(0)}$	200 [Nm]	[29]
Motor Tech	-	PM	[29]
Rotor Inertia	I_{rot}	0.178 [kg m^2]	[29]
Drive Bandwidth	ω_{EM}	180 [rad/s]	≠
Current Capacity	C_{cell}	64 [Ah]	[29]
Efficiency	η_{EM}	0,967 [%]	[29]
Max Speed	$\omega_{EM(max)}$	12800 [rpm]	[29]
Nom.Torque	$Tq_{EM}(\omega_{EM(nom)})$	200 [Nm]	[29]
Pole Pairs	n_P	6	[29]
Fixed gear ratio	k_{rid}	9,59 [%]	[29]
Battery Voltage Nom-Max	$V_{batt(nom)}$-$V_{batt(max)}$	364 [V]-400 [V]	[29]
Battery Weight	M_{batt}	275 [kg]	[29]

For the prescribed benchmark authors considered two different powertrain configurations visible in Figure 9. The first one represented in Figure 9-a (left side) corresponds to a conventional powertrain layout in which a single electrical motor is used to distribute power to frontal wheels through a differential mechanism. Main features of this motor are described in Table III. An alternative powertrain solution with four In-Wheel Motors (IWM) is described in Figure 9-b (right side): in this second case nominal total installed power is the same of the single motor solution. Therefore, the nominal torque exerted by each IWM is a quarter respect to conventional single motor layout. This powertrain configuration is not related to any existing application and it's introduced only to comparatively evaluate the possible advantages arising from different powertrain configurations respect to the conventional one, able in this case to distribute electric and dissipative braking effort independently among all the wheels of a vehicle, whose main mechanical features are inspired to feasible or near to realistic applications.

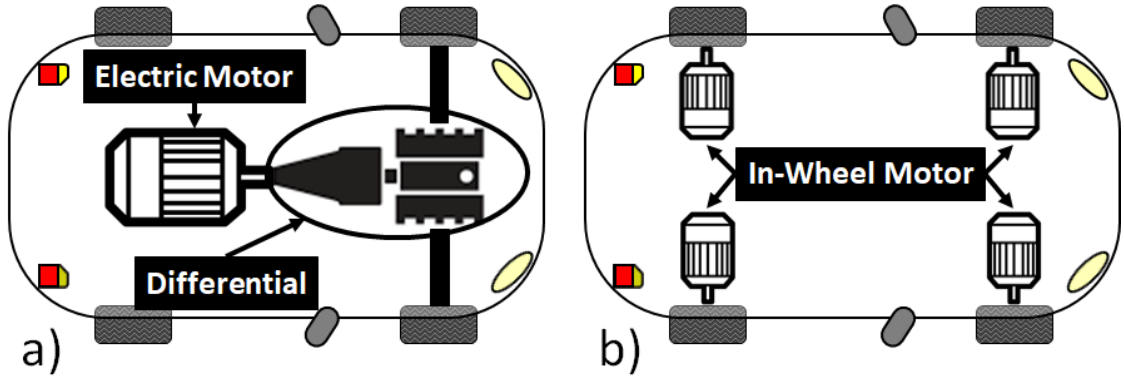

Figure 9 Simulated vehicle powertrain: a) single motor connected to front wheel by a differential mechanism (conventional); b) four in-wheel motor (considering a different motor for each wheel).

Over described model was implemented in MATLAB Simulink™ (release 2018a): each subsystem of the vehicle (i.e. driver, chassis, wheels, electric motor, battery, stability controller, brake unit, etc.) are implemented as an independent model instance, allowing a separate execution of each sub-models with different sampling frequencies and solver features (Figure 10). In this way it's possible to perform a fixed step concurrent execution of each plant in separated tasks, allowing a fast RT execution. Also, execution in

separated threads allow to verify potentially negative drawbacks, in terms of stability, due to delay that necessarily affect the communication between time continuous and discrete systems. A maximum integration frequency of 1 kHz has been chosen in order to make reasonably easy a real time implementation of the proposed model.

In particular, for the vehicle chassis is adopted a planar 3 D.O.F. model (longitudinal and lateral motion with yaw rotation). Also, rotation of each wheel is considered while a Pacejka approach [43] is used to reproduce tyre-road interaction. In particular we adopted the so called "Magic Formula Pure Longitudinal Slip", described by (24).

$$F_{x0} = D_x \sin\left(C_x \tan^{-1}\left[\left\{B_x\kappa_x - E_x\left[B_x\kappa_x - \tan^{-1}\left(B_x\kappa_x\right)\right]\right\}\right]\right) + S_{Vx} \tag{24}$$

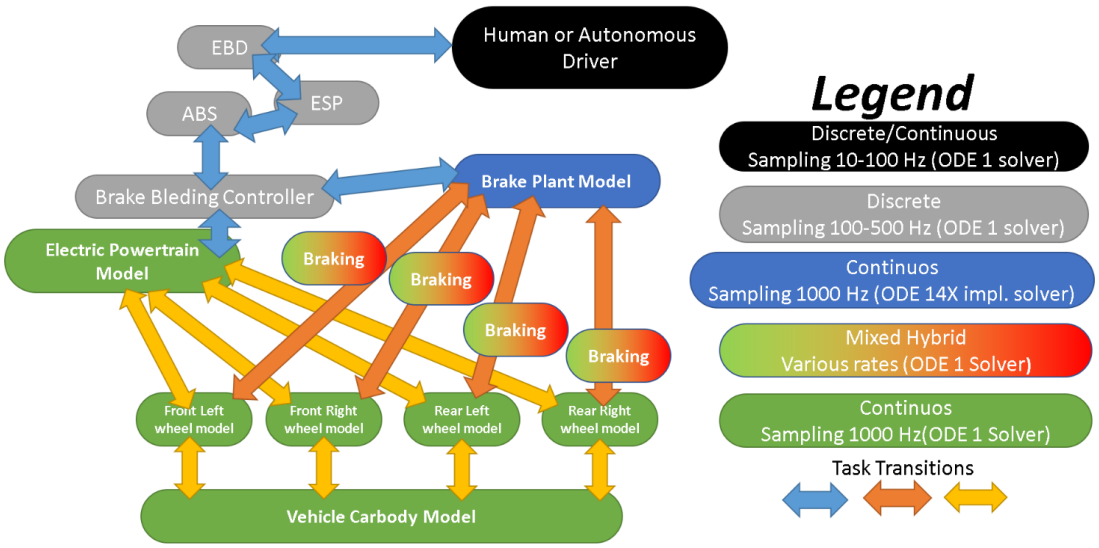

Figure 10 *Multi-thread implementation with corresponding integration frequencies and solvers.*

For high level control sub-systems authors adopted the same simplified logics which are also used by corresponding models available on other commercial software, which apply different torque vectoring techniques. In particular, the following subsystem are implemented according to the Siemens Simcenter Amesim™ (v17.0) stability controller's logic, inspired by [44]:

- EBD (Electronic Brake Distribution): assure a proper repartition of the braking forces respect to the distribution of the normal forces on wheels, according to the longitudinal load transfer.
- ABS/ASR: during the braking phase the ABS (Anti-Blockier System) it's able to optimize the application of longitudinal forces respect to available adhesion condition between road and tires. The same function during the traction phase it's assured by the ASR (Anti-Slip Regulation).
- ESP (Electronic Stability Program): which corrects the longitudinal force applied to the vehicle's wheels in order to assure the directional stability of the vehicle (differential torque applied between left and right wheels).
- Human Driver: simulates the behaviour of a human driver attempting to control the vehicle, in order to perform a known mission profile.

The interchangeability of adopted Simulink™ sub-models respect to corresponding Siemens Amesim™ ones was deliberately chosen in order to make easier integration and co-simulation between the different simulation instruments. This seamless integration between different simulation instruments is a part of the objective of the Obelics Project [45] which have financed this activity. In particular, each system has been designed in order to be easily converted in to a neutral exchange format, the so called FMI (Functional Mock up Interface), which has been the object of a great research interest, especially for mechatronic applications [46], [47].

Preliminary Simulation Results:

Using the over described benchmark model, authors performed some preliminary simulations in order to verify some fundamental features of the brake models introduced in this work, i.e.:

- Brake Blending Controller BBC.
- Brake Plant.
- Braking Units.

Aim of the simulations is not to produce validated results (most of vehicle data are approximated), but to demonstrate that the proposed brake models should be useful employed to evaluate some crucial aspect of the EVs.

Preliminary Results for Brake Blending Controller

Proposed brake blending strategy proved to be very flexible since it was possible to use the same model for both powertrain configurations (visible in Figure 9) proposed for the benchmark test model. Different customization substantially regards model parameters, not functionality aspect.

In Figure 11 an example is shown: a constant braking torque of -700 Nm is demanded to a motorized wheel of the vehicle (referred to the Figure 9-a powertrain layout), from a starting speed of 100 km/h. The algorithm automatically allocate the maximum available braking torque to the electric motor in the respect of its own constraints. If there is a gap between the demanded wheel braking torque and one made available by the regenerative system, the remaining different should be supplied by the friction brake.

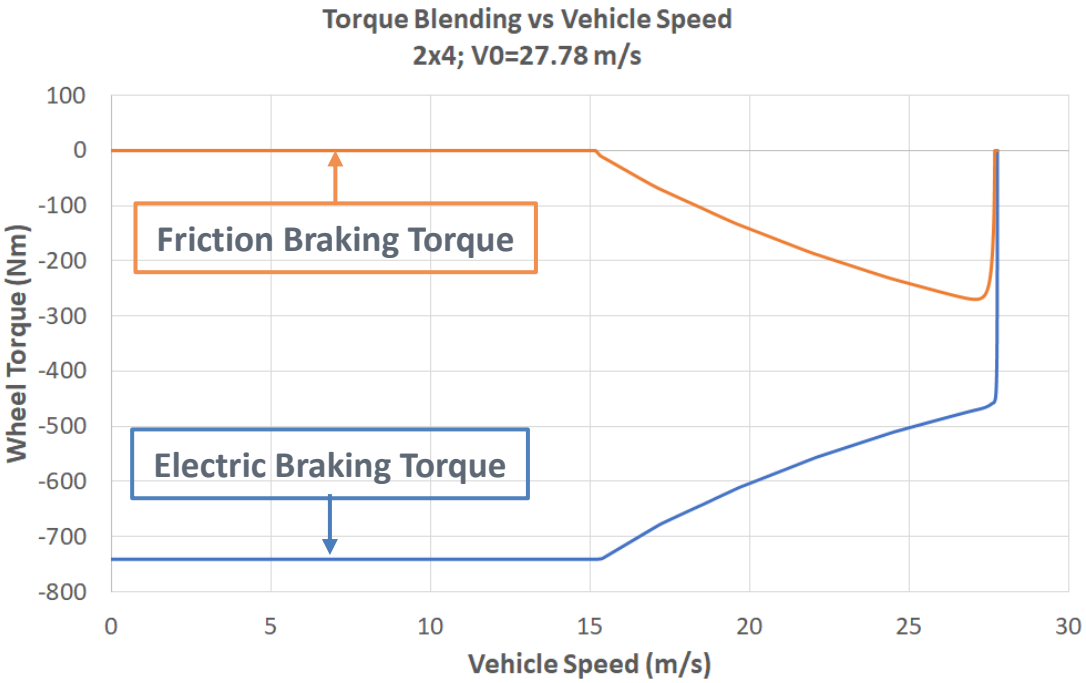

Figure 11 *Torque allocation on motorized wheels during a constant braking manoeuvre.*

Preliminary Results for Brake Plant

In Figure 12 some results regarding the control of the brake callipers are shown: it's simulated the application of a full braking manoeuvre, followed by a modulation pattern due to ABS intervention, with a constant duty cycle of 50%. Proposed model is clearly able to reproduce some typical features of the plant: as example the presence of a finite delay in the response of the calliper, which are clearly influenced by the additional flow request needed to cause the piston motion and to recover compressibility effect. Once the pad, clamped by the calliper, reaches the brake pad surface there is a sudden increase of the clamping pressure and the corresponding exerted brake torques.

When ABS modulation pattern is activated, limited bandwidth of ABS valves and compressibility effects assure a relatively smooth behaviour of applied clamping and braking forces. Therefore, it should be argued that the proposed model, despite to its relative simplicity, is able to reproduce the typical behaviour of a real plant.

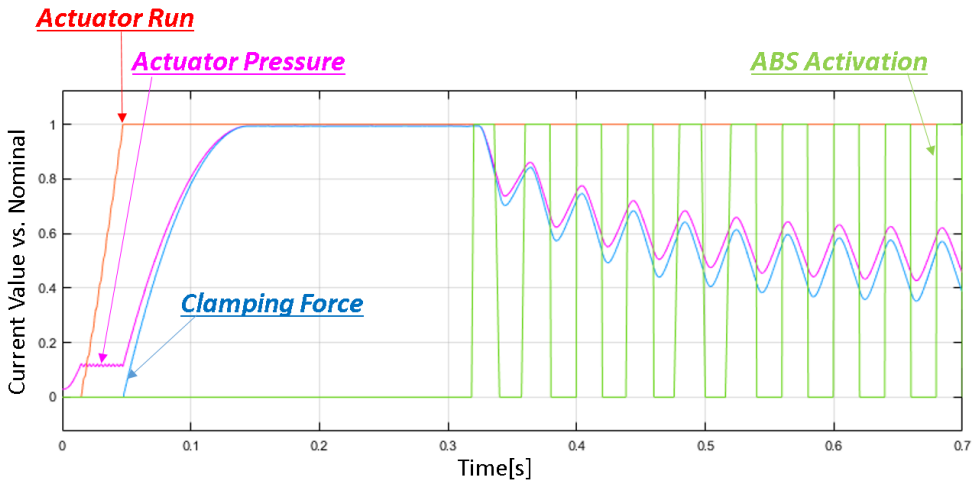

Figure 12 Example of simulated hydraulic response of a brake calliper.

Response of the simulated brake plant can be calibrated respect to real experimental data as they become available. In fact, the shape of the system response can be easily changed by managing some parameters, whose physical comprehension is relatively simple. As visible Figure 13, simulated response of the system can be customized, working on a limited number of parameters:

- Calliper run: represents the run of calliper hydraulic actuation, which simulates the requirement of minimum volume of fluid to produce the desired clamping force. It's very useful to replicate a fixed delay in the plant, without to introducing too much complicated or hard-to-tune dynamics. Increasing the calliper run introduce also a moderate degradation of system bandwidth. This feature is useful to reproduce the fact that the final volume of the simulated plant is slightly increased. For example, in Figure 13 the run is reduced to a half respect to nominal condition, producing, as previously described, a reduction of the delay in terms of calliper response.
- Bulk modulus and compressibility effects: by reducing fluid bulk modulus a higher volume of oil has to be transferred to the calliper to obtain the same response. As consequence, visible in Figure 13, by doubling the consistency of

the compressibility effects, the response of the system is slower. An equivalent reduction of bulk modulus should be used also to take count of elastic compliance of pipes or additional plant dead volumes, that are difficult to exactly evaluated.

- Hydraulic losses: an increase of friction losses in pipes and valves introduce a slower response of the plant, also increasing fixed delays as visible in the example of Figure 13, where these losses are doubled.
- Additional parameters: by slight modifying variables, such as applied preloads and equivalent inertia of the calliper, or frequency response of valves, is possible to further reshape the response of the valve making really simple the customization of the plant respect to available experimental data.

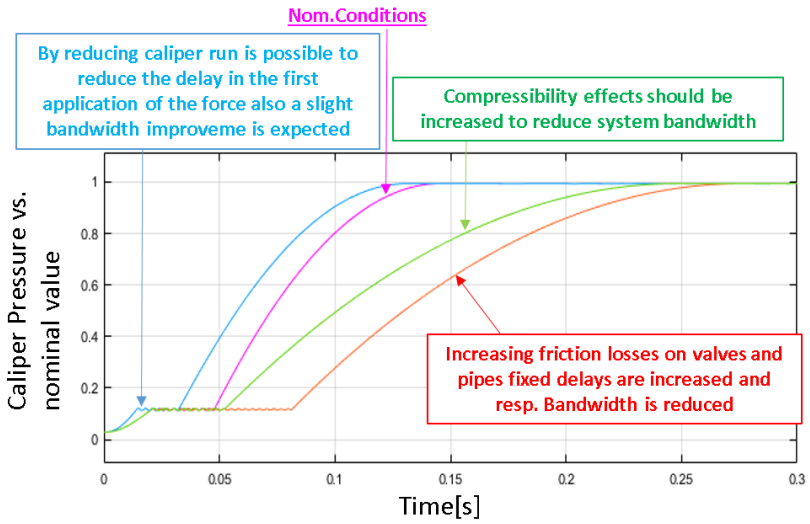

Figure 13 *Response sensitivity of the caliper respect to variation of known input parameters.*

Using the simplified vehicle model described in the previous section, it's also possible to simulate the multiple interactions between braking plant and installed on board subsystems, dedicated to the preservation of the vehicle stability (ABS, ESP, etc.). As example, some simulations of a Double Lane Change (DLC) [47] test have been performed. As visible in TABLE IV, tests were performed by different powertrain layouts of the vehicle and different adherence conditions, considering also the availability of the stability control, performed by the on-board ESP systems. Some results in terms of

maximum speed for which vehicle stability is verified during the DLC manoeuvre are shown: the model highlight the benefit obtained by the application of the ESP control to different powertrain layouts. Model is also able to reproduce the system performances respect to available wheel-road adhesion conditions.

TABLE IV *Double lane change test max speed performed by different vehicles powertrain configurations and adherence coefficient.*

Double Lane Change Simulation Test			
Adherence	*Vehicle Layout*	*ESP*	*Maximum Speed*
0.5	2x4	No	30 km/h
		Yes	35 km/h
	4x4	No	35 km/h
		Yes	45 km/h
0.75	2x4	No	70 km/h
		Yes	75 km/h
	4x4	No	70 km/h
		Yes	80 km/h
1	2x4	No	85 km/h
		Yes	90 km/h
	4x4	No	85 km/h
		Yes	90 km/h

Results in terms of compared vehicle trajectories during a DLC test are shown in Figure 14: simulations are performed considering a traveling speed of 80 km/h and the availability of full adhesion conditions (μ=1). Best performances are obtained by the vehicle equipped with four in-wheel motors and the ESP system able to perform a full torque vectoring of the applied traction efforts.

In Figure 15 instead, results in terms of torque vectoring performed by the ESP controller with four in-wheel motors are shown.

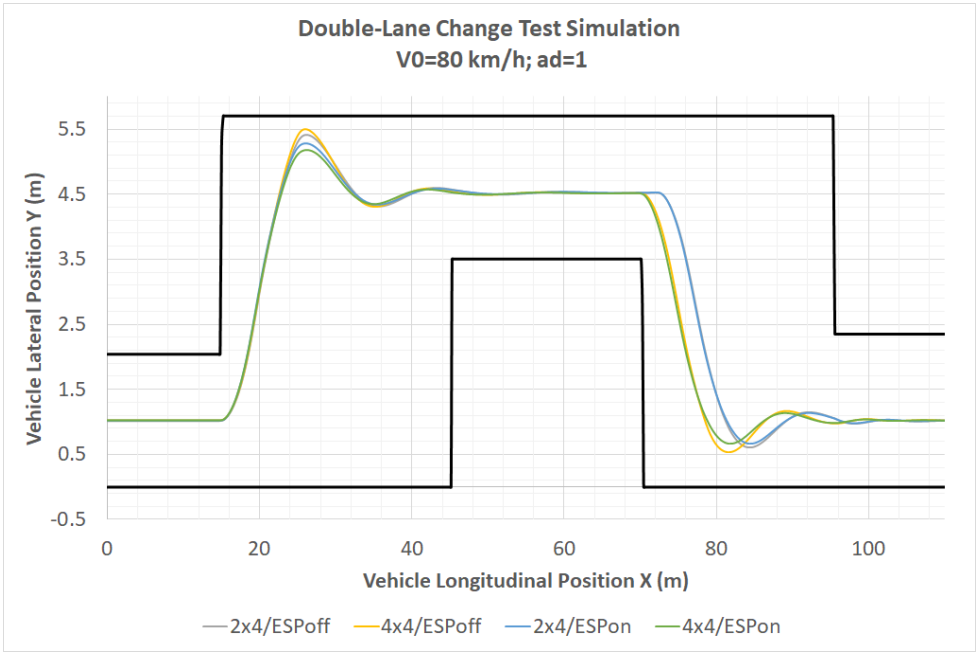

Figure 14 Trajectories of the benchmark vehicle with different powertrain configuration and the availability of the ESP.

Figure 15 Torque vectoring during a DLC test at a constant speed of 80 km/h.

Preliminary Results for the Braking System

Adopting the over-described modular brake models, authors were able to reproduce different mission profiles, which are briefly represented in Figure 16, in order to verify how proposed regeneration strategies applied to different powertrain should affect vehicle performances in terms of saved energy, and consumed volume of brake pads. Authors preferred to verify their simulations on different test cycles [48]–[50] in order to verify robustness of obtained results respect to specific features of simulated mission profiles. The choice of adopting different driving scenario allow, also, to prevent that specific system calibrations, tuned for certain driving cycles, are not robust for different driving situations. This is a matter that has been recently studied also by some of the authors [51] as a part of ASTERICS project [52].

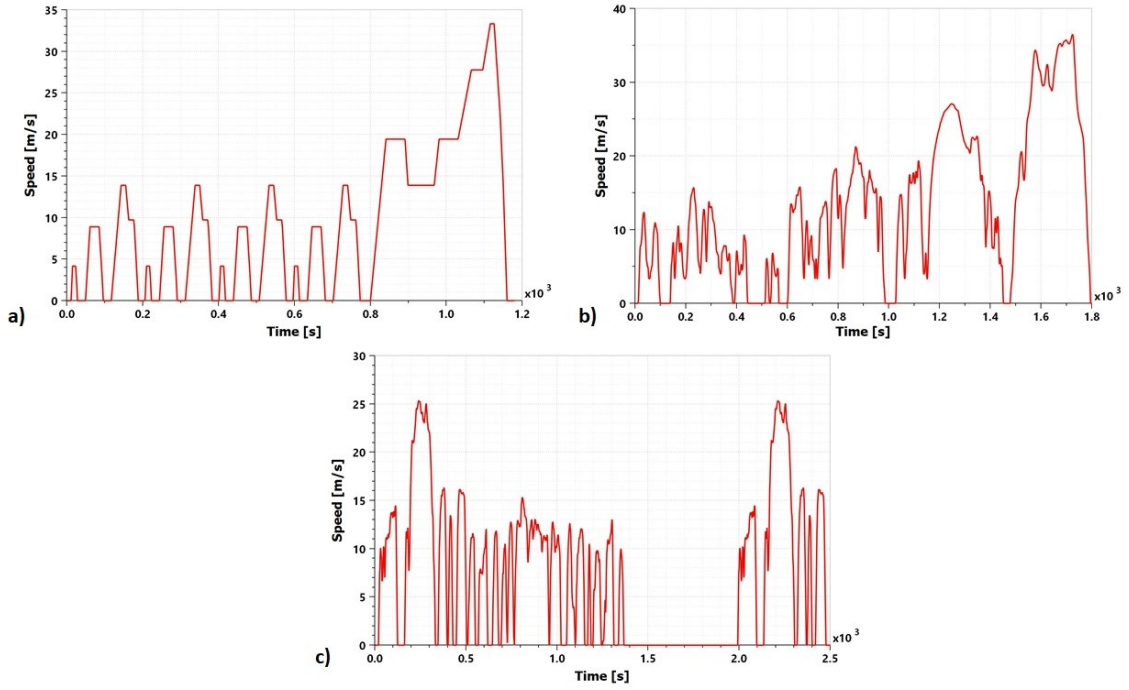

Figure 16 Different simulated driving cycles: a) NEDC; b) WLP Class 3; c) FTP-75.

As visible TABLE V, authors were able to evaluate advantages of applied blending strategies in terms of regenerated energy and reduction of brake pad wear. Results, as expected, confirm that a four-wheel drive vehicle is absolutely desirable in terms of regenerated energy. However, an interesting result is represented by the expected

reduction of brake pad wear, including the corresponding improvement of environmental impact. Results can be easily explained considering the limited decelerations imposed to vehicles on simulated tests, that clearly justify a near to complete regenerative braking for the four in-wheel drive vehicle. It's also interesting to notice that these results have been obtained with the same model by simply adjusting some parameters, without introduce noticeable changes in the overall simulation system.

TABLE V Different consumed and recovered energy for both simulated powertrain configurations

Ref. Drive Cycle	Traction Layout	Recovered vs. Consumed energy	Total Pad Wear Reduction
NEDC	2x4	0,258	About 60%
	4x4	0,427	About 99%
WLTP	2x4	0,287	About 68%
	4x4	0,454	About 99%
FTP-75	2x4	0,393	About 66%
	4x4	0,601	About 99%

Conclusion and Future Developments

In this work authors have presented some preliminary results concerning the development of modular brake models, that offer interesting features for preliminary the sizing and optimization of brake blending policies for electric vehicles, including RTI for fast prototyping of codes, devoted to HIL Simulation. Results presented in this work are mainly referred to a preliminary benchmark test case whose aim is to demonstrate more modelling functionalities than results. Proposed models should be further calibrated and validated as the industrial partners of the project provide some data of the vehicles and corresponding performances in real operating conditions. Results of these further activities should be the object of future publications (obviously respecting Non-Disclosure Agreement signed with the owner of shared data).

Acknowledgements

This work is part of the OBELICS project which has received funding from the European Union Horizon 2020 research and innovation programme under grant agreement No. 769506.

References

[1] A. Emadi, Young Joo Lee, and K. Rajashekara, 'Power Electronics and Motor Drives in Electric, Hybrid Electric, and Plug-In Hybrid Electric Vehicles', *IEEE Transactions on Industrial Electronics*, vol. 55, no. 6, pp. 2237–2245, Jun. 2008.

[2] B. Bilgin and A. Emadi, 'Electric Motors in Electrified Transportation: A step toward achieving a sustainable and highly efficient transportation system', *IEEE Power Electronics Magazine*, vol. 1, no. 2, pp. 10–17, Jun. 2014.

[3] J. de Santiago *et al.*, 'Electrical Motor Drivelines in Commercial All-Electric Vehicles: A Review', *IEEE Transactions on Vehicular Technology*, vol. 61, no. 2, pp. 475–484, Feb. 2012.

[4] A. Walker, M. Galea, C. Gerada, A. Mebarki, and D. Gerada, 'A topology selection consideration of electrical machines for traction applications: towards the FreedomCar 2020 targets', p. 10.

[5] T. J. Nicholson, 'DC & AC traction motors', in *IET Professional Development Course on Electric Traction Systems*, Manchester, UK, 2010, pp. 39–51.

[6] Y. Gao, L. Chen, and M. Ehsani, 'Investigation of the Effectiveness of Regenerative Braking for EV and HEV', SAE International, Warrendale, PA, SAE Technical Paper 1999-01–2910, Aug. 1999.

[7] A. Hatam and A. Khalkhali, 'Simulation and sensitivity analysis of wear on the automotive brake pad', *Simulation Modelling Practice and Theory*, vol. 84, pp. 106–123, May 2018.

[8] K. Stevens and M. Tirovic, 'Heat dissipation from a stationary brake disc, Part 1: Analytical modelling and experimental investigations', *Proceedings of the Institution of Mechanical Engineers, Part C: Journal of Mechanical Engineering Science*, vol. 232, no. 9, pp. 1707–1733, May 2018.

[9] T. Grigoratos and G. Martini, 'Brake wear particle emissions: a review', *Environ Sci Pollut Res*, vol. 22, no. 4, pp. 2491–2504, Feb. 2015.

[10] H. Barosova *et al.*, 'Biological response of an in vitro human 3D lung cell model exposed to brake wear debris varies based on brake pad formulation', *Arch Toxicol*, vol. 92, no. 7, pp. 2339–2351, Jul. 2018.
[11] K. Malachova *et al.*, 'Toxicity and mutagenicity of low-metallic automotive brake pad materials', *Ecotoxicology and Environmental Safety*, vol. 131, pp. 37–44, Sep. 2016.
[12] R. de Castro, R. E. Araújo, M. Tanelli, S. M. Savaresi, and D. Freitas, 'Torque blending and wheel slip control in EVs with in-wheel motors', *Vehicle System Dynamics*, vol. 50, no. sup1, pp. 71–94, Jan. 2012.
[13] S. Di Cairano, H. E. Tseng, D. Bernardini, and A. Bemporad, 'Vehicle Yaw Stability Control by Coordinated Active Front Steering and Differential Braking in the Tire Sideslip Angles Domain', *IEEE Trans. Contr. Syst. Technol.*, vol. 21, no. 4, pp. 1236–1248, Jul. 2013.
[14] L. De Novellis *et al.*, 'Direct yaw moment control actuated through electric drivetrains and friction brakes: Theoretical design and experimental assessment', *Mechatronics*, vol. 26, pp. 1–15, Mar. 2015.
[15] Y. Hori, 'Future vehicle driven by electricity and control-research on four wheel motored "UOT Electric March II"', in *7th International Workshop on Advanced Motion Control. Proceedings (Cat. No.02TH8623)*, Maribor, Slovenia, 2002, pp. 1–14.
[16] Y. Chen, J. K. Hedrick, and K. Guo, 'A novel direct yaw moment controller for in-wheel motor electric vehicles', *Vehicle System Dynamics*, vol. 51, no. 6, pp. 925–942, Jun. 2013.
[17] F. Tahami, S. Farhangi, and R. Kazemi, 'A Fuzzy Logic Direct Yaw-Moment Control System for All-Wheel-Drive Electric Vehicles', *Vehicle System Dynamics*, vol. 41, no. 3, pp. 203–221, Jan. 2004.
[18] Cong Geng, L. Mostefai, M. Denai, and Y. Hori, 'Direct Yaw-Moment Control of an In-Wheel-Motored Electric Vehicle Based on Body Slip Angle Fuzzy Observer', *IEEE Trans. Ind. Electron.*, vol. 56, no. 5, pp. 1411–1419, May 2009.
[19] K. Bayar, J. Wang, and G. Rizzoni, 'Development of a vehicle stability control strategy for a hybrid electric vehicle equipped with axle motors', *Proceedings of the Institution of Mechanical Engineers, Part D: Journal of Automobile Engineering*, vol. 226, no. 6, pp. 795–814, Jun. 2012.
[20] L. Pugi, F. Grasso, M. Pratesi, M. Cipriani, and A. Bartolomei, 'Design and preliminary performance evaluation of a four wheeled vehicle with degraded adhesion conditions', *International Journal of Electric and Hybrid Vehicles*, vol. 9, no. 1, p. 1, 2017.
[21] J. Wang, Q. Wang, L. Jin, and C. Song, 'Independent wheel torque control of 4WD electric vehicle for differential drive assisted steering', *Mechatronics*, vol. 21, no. 1, pp. 63–76, Feb. 2011.
[22] S. Eppler, T. Klenk, and J. Wiedemann, 'Thermal Simulation within the Brake System Design Process', presented at the 20th Annual Brake Colloquium And Exhibition, 2002, pp. 2002-01–2587.
[23] S. R. Cikanek and K. E. Bailey, 'Regenerative braking system for a hybrid electric vehicle', in *Proceedings of the 2002 American Control Conference (IEEE Cat. No.CH37301)*, Anchorage, AK, USA, 2002, pp. 3129–3134 vol.4.
[24] M. Ito, F. Kawahata, M. Ohkubo, K. Nakamura, A. Sakai, and A. Otomo, 'Brake apparatus for an electric vehicle to maximize regenerative energy', US5895100A, 20-Apr-1999.

[25] F. Talati and S. Jalalifar, ‘Analysis of heat conduction in a disk brake system’, *Heat Mass Transfer*, vol. 45, no. 8, pp. 1047–1059, Jun. 2009.
[26] R. Limpert, ‘Brake Design and Safety’, in *Brake Design and Safety*, SAE, 2011, pp. i–xv.
[27] A. Belhocine and M. Bouchetara, ‘Thermal analysis of a solid brake disc’, *Applied Thermal Engineering*, vol. 32, pp. 59–67, Jan. 2012.
[28] D. Savitski *et al.*, ‘The new paradigm of an anti-lock braking system for a full electric vehicle: experimental investigation and benchmarking’, *Proceedings of the Institution of Mechanical Engineers, Part D: Journal of Automobile Engineering*, vol. 230, no. 10, pp. 1364–1377, Sep. 2016.
[29] J. Zhang, C. Lv, J. Gou, and D. Kong, ‘Cooperative control of regenerative braking and hydraulic braking of an electrified passenger car’, *Proceedings of the Institution of Mechanical Engineers, Part D: Journal of Automobile Engineering*, vol. 226, no. 10, pp. 1289–1302, Oct. 2012.
[30] C. Lv, J. Zhang, Y. Li, and Y. Yuan, ‘Regenerative Braking Control Algorithm for an Electrified Vehicle Equipped with a By-Wire Brake System’, presented at the SAE 2014 World Congress & Exhibition, 2014, pp. 2014-01–1791.
[31] C. Lv, J. Zhang, Y. Li, and Y. Yuan, ‘Directional-stability-aware brake blending control synthesis for over-actuated electric vehicles during straight-line deceleration’, *Mechatronics*, vol. 38, pp. 121–131, Sep. 2016.
[32] L. Berzi, T. Favilli, E. Locorotondo, M. Pierini, and L. Pugi, ‘Real Time Models of Automotive Mechatronics Systems: Verifications on “Toy Models”’, in *Advances in Italian Mechanism Science*, vol. 68, G. Carbone and A. Gasparetto, Eds. Cham: Springer International Publishing, 2019, pp. 141–148.
[33] L. Pugi, M. Malvezzi, S. Papini, and S. Tesi, ‘Simulation of braking performance: The AnsaldoBreda EMU V250 application’, p. 13.
[34] C. Satzger and R. de Castro, ‘Combined wheel-slip control and torque blending using MPC’, in *2014 International Conference on Connected Vehicles and Expo (ICCVE)*, Vienna, Austria, 2014, pp. 618–624.
[35] C. Satzger, R. de Castro, A. Knoblach, and J. Brembeck, ‘Design and validation of an MPC-based torque blending and wheel slip control strategy’, in *2016 IEEE Intelligent Vehicles Symposium (IV)*, Gotenburg, Sweden, 2016, pp. 514–520.
[36] L. Pugi, M. Malvezzi, A. Tarasconi, A. Palazzolo, G. Cocci, and M. Violani, ‘HIL simulation of WSP systems on MI-6 test rig’, *Vehicle System Dynamics*, vol. 44, no. sup1, pp. 843–852, Jan. 2006.
[37] G. Genta and L. Morello, Eds., ‘Braking System’, in *The Automotive Chassis: Vol. 1: Components Design*, Dordrecht: Springer Netherlands, 2009, pp. 269–316.
[38] L. Pugi, R. Conti, D. Nocciolini, E. Galardi, A. Rindi, and S. Rossin, ‘A Tool for the Simulation of Turbo-Machine Auxiliary Lubrication Plants’, *International Journal of Fluid Power*, vol. 15, no. 2, pp. 87–100, May 2014.
[39] J. Kukutschová *et al.*, ‘Wear mechanism in automotive brake materials, wear debris and its potential environmental impact’, *Wear*, vol. 267, no. 5–8, pp. 807–817, Jun. 2009.
[40] H.-G. Namgung *et al.*, ‘Size distribution analysis of airborne wear particles released by subway brake system’, *Wear*, vol. 372–373, pp. 169–176, Feb. 2017.
[41] G. Perricone *et al.*, ‘A concept for reducing PM 10 emissions for car brakes by 50%’, *Wear*, vol. 396–397, pp. 135–145, Feb. 2018.
[42] Fiat500USA.com, ‘Fiat 500e Full Vehicle Specifications!’ .
[43] H. Pacejka, *Tire and Vehicle Dynamics*. Elsevier, 2005.

[44] ‘Bosch Automotive Handbook, 10th Edition’. [Online]. Available: https://www.sae.org/publications/books/content/bosch10/. [Accessed: 29-Apr-2019].
[45] ‘Homepage - Obelics | Obelics’. [Online]. Available: https://obelics.eu/. [Accessed: 17-Apr-2019].
[46] T. Blockwitz *et al.*, ‘Functional Mockup Interface 2.0: The Standard for Tool independent Exchange of Simulation Models’, presented at the 9th International MODELICA Conference, Munich, Germany, 2012, pp. 173–184.
[47] International Organization for Standardization, *Passenger Cars--Test Track for a Severe Lane-change Manoeuvre: Part 1: Double Lane-change*. 1999.
[48] Q. Ren, D. A. Crolla, and A. Morris, ‘Effect of transmission design on Electric Vehicle (EV) performance’, in *2009 IEEE Vehicle Power and Propulsion Conference*, Dearborn, MI, 2009, pp. 1260–1265.
[49] J. Demuynck, D. Bosteels, M. De Paepe, C. Favre, J. May, and S. Verhelst, ‘Recommendations for the new WLTP cycle based on an analysis of vehicle emission measurements on NEDC and CADC’, *Energy Policy*, vol. 49, pp. 234–242, Oct. 2012.
[50] M. Montazeri-Gh and M. Naghizadeh, ‘DEVELOPMENT OF CAR DRIVE CYCLE FOR SIMULATION OF EMISSIONS AND FUEL ECONOMY’, p. 6.
[51] L. Berzi, M. Delogu, and M. Pierini, ‘Development of driving cycles for electric vehicles in the context of the city of Florence’, *Transportation Research Part D: Transport and Environment*, vol. 47, pp. 299–322, Aug. 2016.
[52] ‘Asterics - Homepage’. [Online]. Available: http://www.asterics-project.eu/. [Accessed: 02-May-2019].